

Fundamental limits in single-molecule orientation measurements

Matthew R Foreman¹ and Peter Török¹

Blackett Laboratory, Department of Physics, Imperial College London,
Prince Consort Road, London SW7 2BZ, UK

E-mail: matthew.foreman@imperial.ac.uk and peter.torok@imperial.ac.uk

New Journal of Physics **13** (2011) 093013 (20pp)

Received 4 May 2011

Published 7 September 2011

Online at <http://www.njp.org/>

doi:10.1088/1367-2630/13/9/093013

Abstract. Directionality inherent in the polarization of light affords the means of performing robust dynamic orientational measurements of molecules and asymmetric scatterers. In this paper, the precision with which measurements of this kind can be made is quantified for a number of common polarization-based measurement architectures using a metric derived from Fisher information. Specifically, a fundamental limit of 0.5 radian per detected photon (on average) is found, thus highlighting the importance of maximizing photon numbers by correct fluorophore selection. Informational dips, whereby measurement precision is degraded, are shown to arise in many realistic measurement scenarios, particularly for inference from null readings. The severity of these precision losses is therefore considered, and it is shown to decrease with increased system redundancy. Contamination of measured data from coherently and incoherently radiating extraneous sources, furthermore, causes a loss of precision. Analytic and numerical results are hence also presented in this vein.

¹ Authors to whom any correspondence should be addressed.

Contents

1. Introduction	2
2. Theory of polarization-based orientation measurements of a single molecule	3
2.1. Image of an electric dipole	3
2.2. Division-of-amplitude polarimetry	5
3. Precision in orientational measurements	7
3.1. Fisher information	7
3.2. Estimating the transverse dipole orientation	9
3.3. Dipolar crosstalk	12
4. Conclusions	17
Acknowledgment	18
References	18

1. Introduction

The development of techniques such as (fluorescence) photoactivated localization microscopy (PALM and FPALM) and stochastic optical reconstruction microscopy (STORM) [1, 2] has revolutionized super-resolution microscopy in recent years. These methodologies have, in turn, driven scientific advancement in, for example, the study of cell dynamics, atom-based quantum information processing and super-resolution microscopy [3–5]. The measurement of the orientation of single molecules arguably promises equally important gains, since this additional degree of freedom contains further information about the molecule, its micro-environment and history. Orientational measurements have, for instance, allowed conformational changes and structure–function relationships of living cells and proteins to be examined by means of tracking fixed-site fluorescent tags [3, 6, 7]. Furthermore, any angular dependence of physical properties of single molecules, such as state transition probabilities or strong field ionization potential, can provide fundamental insights into the photophysics of molecular sources [8, 9]. Practically, optical measurements of molecular orientation have been achieved using techniques based on structured illumination, defocused image fitting and total internal reflection [10–12]; however, these can often suffer from poor signal-to-noise ratios and restrictive experimental conditions. The inherent directionality of the polarization state of light, however, provides a natural alternative by which to make robust orientational measurements [13, 14]. Accordingly, a number of super-resolution microscopy techniques incorporating polarization have been pursued and reported in the literature [15–17].

The need to fully characterize and benchmark competing localization and imaging systems has motivated much research into relevant performance limits [5, 18, 19]. The quantification of such limits is of importance in terms of both system design, particularly in scenarios with limited photon budgets, and data analysis. Measurement limits in orientational studies are similarly relevant; however, conventional performance metrics, such as signal-to-noise ratios and resolution, are less appropriate in a polarization domain, since they refer to irradiance measurements. We have, however, recently applied informatic and statistical principles to describe the achievable measurement precision in polarization measurements [20]. An extension of that work is presented in this paper, whereby precision limits on the estimation of the orientation of single molecules are presented. While in many practical scenarios fluorophores are able to rotate during an experimental measurement, attention is restricted to rigidly fixed

molecules in this work. Rotational dynamics of a fluorophore give rise to a loss in obtainable precision, as has been considered in [21], meaning that the precision limit derived in this paper represents the best case scenario.

Single-molecule localization can achieve a localization accuracy of a few nanometres; however, such methodologies fail to yield reliable results if multiple fluorescent molecules that are present within the detection volume emit simultaneously. Typically, large errors can arise in such instances since the fitting algorithms commonly used assume *a priori* that only a single molecule is present; however, additional molecules constitute a further noise source, hence affecting achievable precision [19]. Various approaches to overcome the former issue have been proposed and demonstrated in localization microscopy, such as analysis of photobleaching steps or photon statistics [22, 23]; however, the latter is more difficult to overcome. Orientational measurements can similarly suffer from contamination of the measured signal with a resulting loss of inference precision when multiple molecules are present. The severity of this degradation is hence also investigated in this work.

Within this context, section 2.1 first recalls the results pertaining to the imaging of single molecules, while section 2.2 presents the principles of polarization measurements suitable for dynamic orientation studies. The mathematical framework by which the precision of orientational measurements can be quantified is then briefly introduced in section 3.1. These preliminary sections are included for completeness and as a vehicle to define the requisite notation. Section 3.2 draws from earlier sections to establish limits on polarization-based orientational measurements of single molecules; section 3.3 concludes by considering the reduction in measurement precision arising from what is termed ‘dipolar crosstalk’.

2. Theory of polarization-based orientation measurements of a single molecule

2.1. Image of an electric dipole

Fluorescent molecules predominantly radiate due to electric dipole transitions of constituent electrons. As such, an electric dipole emitter is used to model the radiation pattern of a single molecule throughout this text. In microscopy contexts, however, the field radiated from a dipole source must practically be imaged onto a detector. Such an imaging system serves not only to collect emitted light, but also to magnify the object so as to form an image on a usable scale. The modelling and analysis of orientation measurements hence first necessitate the determination of the field distribution in the image plane of an imaging system due to the presence of a dipole in object space. Limitation is made in this work to a simple $4f$ transmission geometry, as shown in figure 1, comprising two lenses of focal lengths f_1 and f_2 , respectively, placed such that they share a common focal plane. Asserting that the imaging system is telecentric, as holds for the vast majority of microscopes, a vectorial ray tracing formulation can be used. See [24–26] for further details of this theory; here it suffices to state that the electric field at a position $\boldsymbol{\rho}_2 = (\rho_2, \varphi_2, z_2)$ relative to the geometric focus of the detector lens (assumed to be in air for simplicity and with numerical aperture (NA) $\sin \alpha_2$) arising from an on-axis, in focus, electric dipole with moment $\mathbf{p} = (p_x, p_y, p_z)$ is given by

$$\mathbf{E}_2(\boldsymbol{\rho}_2) = \begin{pmatrix} p_x(K_0^A + K_2^A \cos 2\varphi_2) + p_y K_2^A \sin 2\varphi_2 + 2ip_z K_1^A \cos \varphi_2 \\ p_x K_2^A \sin 2\varphi_2 + p_y(K_0^A - K_2^A \cos 2\varphi_2) + 2ip_z K_1^A \sin \varphi_2 \\ -2i(p_x \cos \varphi_2 + p_y \sin \varphi_2)K_1^B - 2p_z K_0^B \end{pmatrix}, \quad (1)$$

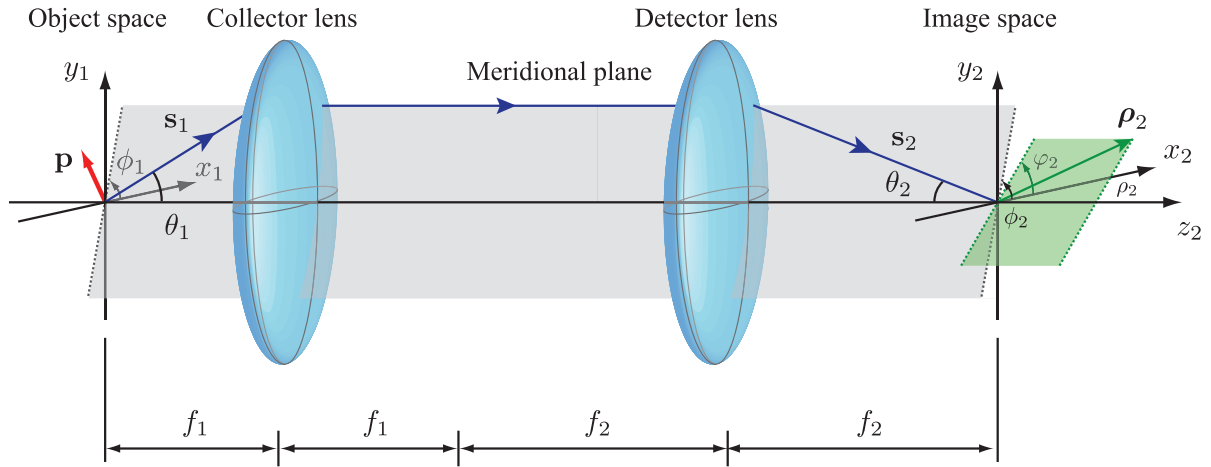


Figure 1. The $4f$ telecentric imaging setup used for imaging a single dipole emitter. Positions in the object and image plane are defined by the position vectors ρ_1 and ρ_2 , respectively, while positions on the reference spheres associated with the collector and detector lens (assumed aplanatic and with numerical apertures $\text{NA}_1 = \sin \alpha_1$ and $\text{NA}_2 = \sin \alpha_2$) are defined by the coordinates (θ_1, ϕ_1) and (θ_2, ϕ_2) . Ray directions in the respective spaces are described by the normalized wavevectors s_1 and s_2 .

where

$$\begin{aligned}
 K_0^A &= \int_0^{\alpha_2} \sqrt{\frac{\cos \theta_2}{\cos \theta_1}} \sin \theta_2 (1 + \cos \theta_1 \cos \theta_2) J_0(k\rho_2 \sin \theta_2) \exp[ikz_2 \cos \theta_2] d\theta_2, \\
 K_0^B &= \int_0^{\alpha_2} \sqrt{\frac{\cos \theta_2}{\cos \theta_1}} \sin^2 \theta_2 \sin \theta_1 J_0(k\rho_2 \sin \theta_2) \exp[ikz_2 \cos \theta_2] d\theta_2, \\
 K_1^A &= \int_0^{\alpha_2} \sqrt{\frac{\cos \theta_2}{\cos \theta_1}} \sin \theta_2 \sin \theta_1 \cos \theta_2 J_1(k\rho_2 \sin \theta_2) \exp[ikz_2 \cos \theta_2] d\theta_2, \\
 K_1^B &= \int_0^{\alpha_2} \sqrt{\frac{\cos \theta_2}{\cos \theta_1}} \sin^2 \theta_2 \cos \theta_1 J_1(k\rho_2 \sin \theta_2) \exp[ikz_2 \cos \theta_2] d\theta_2, \\
 K_2^A &= \int_0^{\alpha_2} \sqrt{\frac{\cos \theta_2}{\cos \theta_1}} \sin \theta_2 (1 - \cos \theta_1 \cos \theta_2) J_2(k\rho_2 \sin \theta_2) \exp[ikz_2 \cos \theta_2] d\theta_2
 \end{aligned} \tag{2}$$

and $J_n(x)$ denotes the Bessel function of the first kind of order n . $k = 2\pi/\lambda$ is the wavenumber of the light radiated by the dipole, assumed to be monochromatic. Numerical evaluation of these integrals requires the use of the aplanatic condition $\sin \theta_1 = (f_2/f_1)\sin \theta_2$, where the ratio $\beta = f_2/f_1$ defines the magnification of the imaging system. Assuming henceforth that the dipole moment of the source lies in a plane perpendicular to the optical axis, as described by

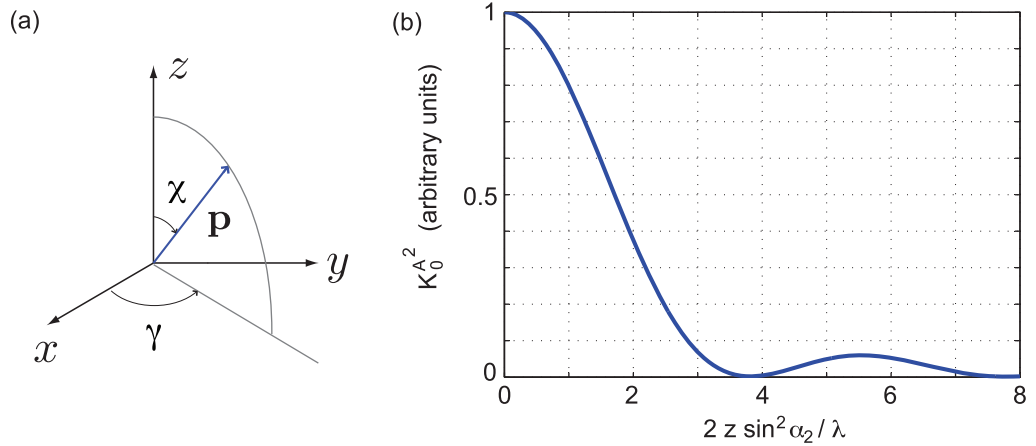


Figure 2. (a) An electric dipole of moment \mathbf{p} has a transverse and longitudinal orientation defined by angles γ and χ , respectively. (b) Variation of $K_0^{A^2}$ with defocus distance z_2 , reflecting the reduction of angular precision with defocus, when using a crossed polarizer polarimeter.

$p_x = p_0 \cos \gamma$, $p_y = p_0 \sin \gamma$ and $p_z = 0$ (see figure 2, with $\chi = \pi/2$), equation (1) reduces to

$$\mathbf{E}_2(\boldsymbol{\rho}_2) = p_0 \begin{pmatrix} (K_0^A + K_2^A \cos 2\varphi_2) \cos \gamma + K_2^A \sin 2\varphi_2 \sin \gamma \\ K_2^A \sin 2\varphi_2 \cos \gamma + (K_0^A - K_2^A \cos 2\varphi_2) \sin \gamma \\ -2iK_1^B (\cos \varphi_2 \cos \gamma + \sin \varphi_2 \sin \gamma) \end{pmatrix}. \quad (3)$$

Equation (3) demonstrates the inherent relationship between the polarization state of the field in the image plane and the orientation γ of the radiating dipole. Hence, polarization, as claimed, provides a natural property of light from which molecular orientation can be determined. The next section therefore focuses on how such polarization-based measurements can be made and described.

2.2. Division-of-amplitude polarimetry

A number of different detection architectures exist that are capable of measuring the state of polarization of light. For example, nulling techniques operate by passing light through variable analysers which are adjusted in an attempt to fully extinguish the light [27]. Nulling techniques are, however, less suitable for the study of dynamic systems, due to the long acquisition times and low light efficiency involved. In contrast, division-of-amplitude polarimetry, in which light is split and each resulting beam simultaneously analysed, allows rapid data acquisition with high light efficiency. For example, the four Si detector polarimeter of Azzam [28] is theoretically 100% light efficient, as too is the polarimeter of Lara and Paterson [29] described below. The intensity D_i on the i th detector can be found by forming the inner product of the input Stokes vector $\mathbf{S} = (S_0, S_1, S_2, S_3)^T$ with a measurement vector $\mathbf{T}_i = (1, T_{1i}, T_{2i}, T_{3i})^T/2$ (normalized such that $T_{1i}^2 + T_{2i}^2 + T_{3i}^2 = 1$ to ensure a passive system), determined by the analyser configuration. A horizontal polarizer, for example, has an associated measurement vector of

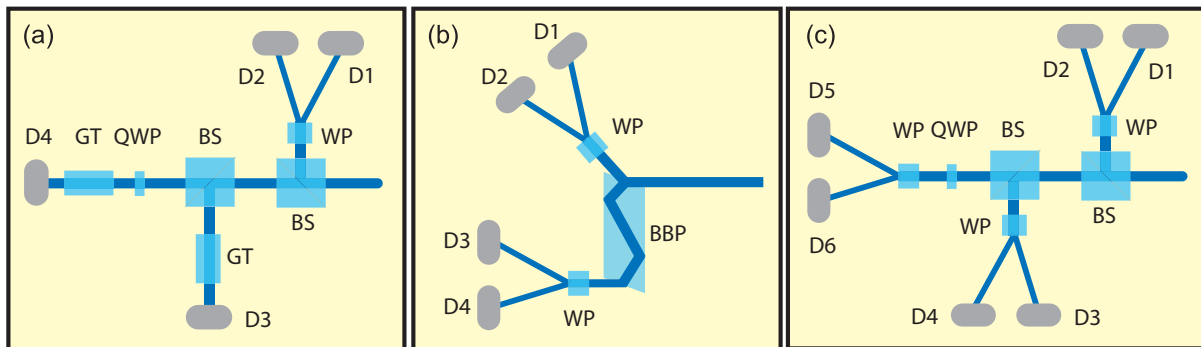


Figure 3. Schematics of three alternative polarimeter designs (see text). The notation is as follows: BS, beam splitter; WP, Wollaston prism; QWP, quarter wave plate; GT, Glan Thompson polarizer; BBP, broadband prism; D, detector.

$(1, 1, 0, 0)/2$. Practically, input light is analysed using at least four distinct analysers, so as to ensure that determination of the polarization state is well conditioned in a noise-free case [20]. The whole measurement process can hence be described using the matrix equation

$$\mathbf{D} = \frac{1}{N} \mathbb{T} \mathbf{S}, \quad (4)$$

where \mathbb{T} is the so-called instrument matrix whose rows correspond to the measurement vector of each analysing state. N is the number of analysing measurements made. It should be noted that it has been assumed that each analyser is illuminated by equal fractions of the total incident intensity, since it has been previously shown that this helps to produce optimal noise characteristics in the inversion problem [20].

A number of polarimeter configurations will be considered in this paper for illustrative purposes and are introduced here for convenience. The first configuration, proposed by Azzam in 1982, is commonly found in the literature due to its conceptual simplicity [30]. In Azzam's design, incident light is projected onto horizontal, vertical, linear 45° and right circular polarized states as can be achieved using the arrangement of polarizers and a quarter-wave plate shown in figure 3(a). The corresponding instrument matrix is thus given by

$$\mathbb{T}_1 = \frac{1}{2} \begin{pmatrix} 1 & 1 & 0 & 0 \\ 1 & -1 & 0 & 0 \\ 1 & 0 & 1 & 0 \\ 1 & 0 & 0 & 1 \end{pmatrix}. \quad (5)$$

Compain and Drevillon [31] proposed an alternative polarimeter architecture (figure 3(b)) in which total internal reflections within a prism are used to introduce the necessary retardance to analyse elliptical states of polarization. Specifically, the geometry of the prism is chosen to minimize the condition number of the instrument matrix (which quantifies noise amplification in the solution of the inverse problem) to a value of 4.48. While the instrument matrix, in general,

depends on the wavelength of the incident light, it is taken here as

$$\mathbb{T}_2 = \frac{1}{2} \begin{pmatrix} 1 & -0.575 & 0.818 & 0 \\ 1 & -0.575 & -0.818 & 0 \\ 1 & 0.617 & -0.003 & 0.787 \\ 1 & 0.617 & 0.003 & -0.787 \end{pmatrix}, \quad (6)$$

where slight power imbalances, of the order of $\sim 5\%$ in each detection arm, are neglected to allow fairer comparison. Figure 3(c) shows a third polarimeter, recently proposed by Lara and Paterson [29], employing six distinct measurement states and described by the instrument matrix

$$\mathbb{T}_3 = \frac{1}{2} \begin{pmatrix} 1 & 1 & 0 & 0 \\ 1 & -1 & 0 & 0 \\ 1 & 0 & 1 & 0 \\ 1 & 0 & -1 & 0 \\ 1 & 0 & 0 & 1 \\ 1 & 0 & 0 & -1 \end{pmatrix}. \quad (7)$$

This polarimeter was shown to possess polarization-independent noise characteristics, in the presence of Gaussian thermal noise and signal-dependent Poisson noise.

Each of these polarimeters is capable of measuring the full state of polarization of input light and, hence, it is possible to infer the orientation of the molecule. The estimation algorithm adopted, however, will in general depend on where, and how many, positions are sampled in image space. Full discussion of possible estimation algorithms is beyond the scope of this paper; however, it is possible to determine fundamental limits on their precision, as shall be discussed in the next section. A discussion of the light efficiency of each of these polarimeters can be found in [20].

It is worthwhile to note that in many fields orientational studies of single molecules are based on determining the fluorescence anisotropy or fluorescence polarization (see, e.g., [32, 33]). Such studies derive from measurements of crossed polarized components of the output field and hence a rudimentary polarimeter is required. Accordingly, crossed polarizers will also be considered throughout this paper. Unique determination of the full polarization state of light is, however, not possible with crossed polarizers and, as a result, important information can be lost. It is for this reason that full polarimetric studies on single molecules can be of interest [13, 34–36].

3. Precision in orientational measurements

3.1. Fisher information

Noise present in a system introduces uncertainty about the true value of a quantity of interest, whether it is the measured quantity itself, such as optical intensity, or a derived quantity, such as molecular orientation. Accordingly, it is necessary to make an estimate, or ‘best guess’, as to the true value of the quantity of interest. The well-known Cramér–Rao lower bound (CRLB) [37, 38] quantifies the precision of any estimate, \hat{w} , of a parameter w , such that the variance of the estimator, K_w , is bounded by $K_w \geq J_w^{-1}$. Here J_w is known as the Fisher information [39],

defined by

$$J_w = E \left[\left(\frac{\partial \ln f_X(x|w)}{\partial w} \right)^T \frac{\partial \ln f_X(x|w)}{\partial w} \right], \quad (8)$$

where $f_X(x|w)$ is the probability density function describing the likelihood that the measured random variable X takes the value x , as will in general depend on the value of w . $E[\dots]$ denotes a statistical expectation over all possible values of x . A multivariate generalization, allowing for multiple measurements \mathbf{X} and estimated parameters \mathbf{w} , can also be defined such that the covariance matrix of the estimate of \mathbf{w} is lower bounded by the inverse of a Fisher information matrix (FIM)

$$\mathbb{J}_w = E \left[\left(\frac{\partial \ln f_{\mathbf{X}}(\mathbf{x}|\mathbf{w})}{\partial \mathbf{w}} \right)^T \frac{\partial \ln f_{\mathbf{X}}(\mathbf{x}|\mathbf{w})}{\partial \mathbf{w}} \right], \quad (9)$$

that is, $\mathbb{K}_w \geq \mathbb{J}_w^{-1}$.

In a microscopy context, intensity measurements are made (i.e. $\mathbf{X} = \mathbf{D}$), the true value of which is dependent on the domain from which light originates on the object, Ω_{ob} , and the spatial extent of the detector Ω_{im} , as expressed by the integral

$$D_i(\Omega_{\text{im}}, \Omega_{\text{ob}}) = \iint_{\Omega_{\text{im}}} D_{\text{im}}^{(i)}(\boldsymbol{\rho}_2, \Omega_{\text{ob}}) d\boldsymbol{\rho}_2. \quad (10)$$

Here $D_{\text{im}}^{(i)}(\boldsymbol{\rho}, \Omega_{\text{ob}})$ is the intensity at a point $\boldsymbol{\rho}_2$ in the detector/image plane due to light originating from Ω_{ob} . Assuming the detector to be corrupted by shot noise, the results of [20] can be used, whereby the FIM associated with the estimation of the parameter vector \mathbf{w} from a set of N intensity measurements $\mathbf{D} = (D_1, D_2, \dots, D_N)$ is

$$\mathbb{J}_w(\Omega_{\text{im}}, \Omega_{\text{ob}}) = \frac{\partial \mathbf{D}^\dagger}{\partial \mathbf{w}} \mathbb{J}_D \frac{\partial \mathbf{D}}{\partial \mathbf{w}}, \quad (11)$$

where

$$\mathbb{J}_D = \frac{1}{h\nu} \text{diag} \left[\frac{1}{D_i + D_{ib}} \right], \quad (12)$$

and a potential background intensity, D_{ib} , has been included. As is the usual convention, $h\nu$ represents the energy of a single photon.

Acquisition of an image, however, means that measurements are made for different domains. For example, an image can be built up in a confocal microscope by scanning the object position, hence changing Ω_{ob} between image points. Measurements from different positions can be stacked into a vector format and equation (11) used; however, the assumption that the noise at each measurement position is independent allows simplification such that the dimensions of \mathbf{D} are greatly reduced, hence facilitating numerical computations. Specifically, it can be shown that Fisher information is additive for independent measurements [40], whereby the total FIM, \mathbb{J}_T , can be found by summing that obtained from each measurement, i.e.

$$\mathbb{J}_T = \sum_k \mathbb{J}_w(\Omega_{\text{im}}^k, \Omega_{\text{ob}}^k), \quad (13)$$

where Ω_{im}^k and Ω_{ob}^k denote the respective domains for each scan point.

3.2. Estimating the transverse dipole orientation

Evaluation of the precision with which the orientation of single molecules can be found first requires determination of the appropriate FIM. Restriction is made throughout this text to determining the orientation of the emission dipole moment. Measurements of the absorption moment are not considered, since if the molecule is not rigidly fixed the emission moment and absorption moment need not correspond, which can lead to further precision losses (see, e.g., [21]). Initially restricting attention to on-axis detection with a point polarimetric detector, equation (1) reduces to $\mathbf{E}_2(\boldsymbol{\rho}_2 = \mathbf{0}) = (K_0^A p_x, K_0^A p_y, 0)^T$. Equivalently the on-axis, in-focus Stokes vector is given by $\mathbf{S}(\boldsymbol{\rho}_2 = \mathbf{0}) = (K_0^{A^2} p_0^2, K_0^{A^2} p_0^2 \cos 2\gamma, K_0^{A^2} p_0^2 \sin 2\gamma, 0)^T$. Inference of the dipole orientation unfortunately requires the estimation of the intensity of the incident light, $S_0 = K_0^{A^2} p_0^2$; accordingly, the FIM for the estimation of the parameter vector $\mathbf{w} = (S_0, \gamma)^T$ must be considered. From equations (4) and (11), it follows that

$$\mathbb{J}_{\mathbf{w}} = \frac{1}{N^2} \frac{\partial \mathbf{S}^T}{\partial \mathbf{w}} \mathbb{T}^T \mathbb{J}_D \mathbb{T} \frac{\partial \mathbf{S}}{\partial \mathbf{w}}, \quad (14)$$

where

$$\frac{\partial \mathbf{S}}{\partial \mathbf{w}} = \begin{pmatrix} 1 & 0 \\ \cos 2\gamma & -2S_0 \sin 2\gamma \\ \sin 2\gamma & 2S_0 \cos 2\gamma \\ 0 & 0 \end{pmatrix}. \quad (15)$$

As described in [20], the intensity can be treated as a nuisance parameter and the reduced Fisher information pertaining to the estimation of the dipole orientation can then be found. Bearing in mind the form of $\mathbf{E}_2(\boldsymbol{\rho}_2 = \mathbf{0})$, perhaps the most intuitive approach to measurement of the dipole orientation is to use a pair of polarizers with the corresponding instrument matrix² given by

$$\mathbb{T} = \frac{1}{2} \begin{pmatrix} 1 & \cos 2\vartheta_1 & \sin 2\vartheta_1 & 0 \\ 1 & \cos 2\vartheta_2 & \sin 2\vartheta_2 & 0 \end{pmatrix}, \quad (16)$$

where ϑ_i define the azimuthal angles of the analysing states. This approach is also justifiable since, by the model and assumptions described above, it is known *a priori* that the light incident onto the detector is fully linearly polarized [41]. From equations (12) and (14)–(16), the Fisher information J_γ can then be explicitly found, neglecting for the moment the background intensity term, to be

$$J_\gamma = \frac{2S_0}{h\nu} \frac{\sin^2(\vartheta_1 - \vartheta_2)}{\cos^2(\gamma - \vartheta_1) + \cos^2(\gamma - \vartheta_2)}. \quad (17)$$

Maximum Fisher information is thus achieved when $\vartheta_1 = \vartheta_2 + \pi/2$, i.e. when the polarizers are crossed, whereupon equation (17) simplifies to $J_\gamma = J_\gamma^{\max} = 2S_0/h\nu$ for all dipole orientations. Noting that S_0 represents the total detected intensity, J_γ^{\max} is seen to vary linearly with the number of photons. Upon invoking the CRLB a precision of 0.5 radian per photon is therefore found to be achievable on average. The importance of photon budget in orientational measurements can then be highlighted by contrasting GFP and Cy5 molecules, which are both commonly used as fluorescent tags in techniques such as PALM and STORM. For example,

² Two measurements are required such that the resulting set of linear equations are well conditioned (neglecting ambiguity as to which quadrant the dipole lies in) when noise is absent.

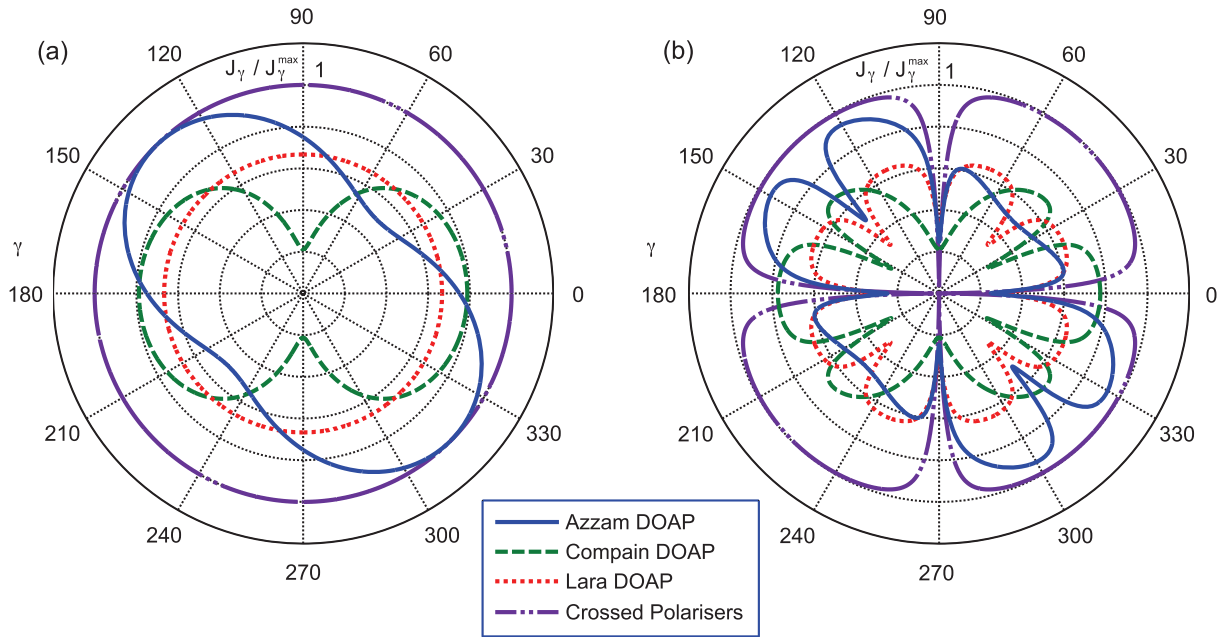


Figure 4. Polar plots, showing the calculated Fisher information $J_\gamma(\gamma)/J_\gamma^{\max}$, for the estimation of the transverse orientation γ of a single electric dipole, for zero background intensity (a) and for $S_0/D_b = 10^3$ (b). Informational dips are introduced in the presence of a background count. The longitudinal angle χ is assumed to be $\pi/2$ and the dipole is assumed to be imaged using a simple $4f$ system with $100\times$ magnification, in which the collector lens has an NA of 0.95 and measured by on-axis polarimeters configured as in section 2.2.

typically 3000 photons can be collected from a single GFP molecule before irreversible photobleaching, yielding an orientational precision of 34.4 arcseconds, while Cy5 photobleaches after approximately 10 000 excitations [19], such that a precision of 10.3 arcseconds can be achieved in the best case. Resistance of fluorophores to photobleaching is, hence, beneficial in terms of achievable accuracy; however, such considerations must naturally be balanced with other experimental factors, such as toxicity and emission wavelengths. An exhaustive comparison of fluorescent dyes is beyond the scope of this paper; however, considerable relevant published data are available (e.g. <http://www.invitrogen.com>). To further maximize the measurement precision design of efficient optical paths, the use of high-quality detectors is also crucial.

It is also informative to consider the Fisher information J_γ when S_0 is assumed to be known *a priori*. In particular for two arbitrarily oriented polarizers, the resulting expression is

$$J_\gamma = J_\gamma^{\max} [\sin^2(\gamma - \vartheta_1) + \sin^2(\gamma - \vartheta_2)], \quad (18)$$

which again reduces to $J_\gamma = J_\gamma^{\max}$ for all dipole orientations, when the polarizers are crossed³. This behaviour has been shown in figure 4(a) in conjunction with the results obtained when

³ While the notation J_γ^{\max} will be retained, it should be observed that when S_0 is known *a priori*, the maximum Fisher information is $2J_\gamma^{\max}$.

the polarimeters introduced in section 2.2 are used to measure the state of polarization on axis, in focus. The improved and γ -independent performance of the crossed polarizer arrangement is evident. This behaviour arises since the polarimeters of section 2.2 are designed for the measurement of the ellipticity, in addition to the azimuthal angle of a state of polarization. Furthermore, the polarimeters of section 2.2 possess more detection arms (see [42]), albeit they can fully determine which quadrant γ lies in.

A defocus in the imaging system, or equivalently an axial shift in the position of the dipole, can also be characterized since the axial coordinate appears only in the K integrals⁴. The variation of $K_0^{A^2}$, and hence J_γ , as a function of defocus distance z_2 is shown in figure 2(b). Oscillatory behaviour is exhibited; however, the best performance is seen within the depth of focus of the imaging system, as would be expected.

Presence of a background intensity during the measurement process, however, produces some interesting behaviour and breaks the orientation independence of the Fisher information, as shall now be considered. Maintaining the assumption that S_0 is known *a priori* for simplicity, when a background intensity D_b is incorporated (assumed the same on each detector), equation (18) becomes

$$J_\gamma = J_\gamma^{\max} \left[\frac{S_0 \sin^2(\gamma - \vartheta_1) \cos^2(\gamma - \vartheta_1)}{S_0 \cos^2(\gamma - \vartheta_1) + D_b} + \frac{S_0 \sin^2(\gamma - \vartheta_2) \cos^2(\gamma - \vartheta_2)}{S_0 \cos^2(\gamma - \vartheta_2) + D_b} \right]. \quad (19)$$

Assuming the polarizers are crossed at angles of 0° and 90° , respectively, gives

$$J_\gamma = J_\gamma^{\max} S_0 \sin^2 \gamma \cos^2 \gamma \left[\frac{1}{S_0 \cos^2 \gamma + D_b} + \frac{1}{S_0 \sin^2 \gamma + D_b} \right]. \quad (20)$$

While in the absence of a background count a constant Fisher information was seen, if the limits $\gamma \rightarrow 0^\circ$ and $\gamma \rightarrow 90^\circ$ are taken, equation (20) yields zero Fisher information, as shown in figure 4(b) (assuming the ratio $S_0/D_b = 10^3$). Dipole orientations that differ from these critical orientations, however, still approximately exhibit the γ invariant behaviour of J_γ . Furthermore, it is found that as the ratio S_0/D_b decreases the width of the information dip around the critical angles increases to such an extent that for large D_b , $J_\gamma \propto \sin 2\gamma$. For reference, it is noted that this is of the same functional form as when Gaussian noise is assumed.

An explanation of this behaviour can be found by first considering inference of the orientation of a dipole using only a single polarizer. The Fisher information in this case is given by a single term of equation (20). Inference from a single polarizer centres around Malus' law with zero intensity corresponding to a dipole orientation perpendicular to the polarizer, while parallel orientations give maximum intensity. The scaling of the variance of Poisson noise with the mean, however, automatically implies that zero intensity suffers no noise, such that it can be identified exactly, while the converse holds for maximum intensity. Furthermore, Malus' law means that small changes in the orientation of a dipole aligned close to these critical orientations give rise to very small changes in the measured intensity (mathematically $\partial D/\partial \gamma = 0$ when the dipole and polarizer are co- or perpendicularly oriented). Due to low noise levels for a perpendicularly oriented dipole, small changes in its orientation can be distinguished.

⁴ The K integrals of equations (2) accommodate a defocus of the detector in the image plane. If, however, the dipole suffers an axial shift, z_{dp} , the exponential term $\exp[ikz_2 \cos \theta_2]$ must be modified to $\exp[ik(z_2 \cos \theta_2 - z_{\text{dp}} \cos \theta_1)]$ (see [43]).

If, however, a dipole is originally parallel to the polarizer, the small intensity changes associated with small rotations are lost in the noise.

Fisher information, being a local measure of information, quantifies the sensitivity of the recorded intensities on the dipole orientation and hence a single polarizer oriented at 0° yields zero Fisher information with regard to a dipole oriented at $\gamma = 0^\circ$, but provides maximum information for $\gamma = 90^\circ$. Thus, if two crossed polarizers are used, a reduction in Fisher information from a measurement in one is counterbalanced by a gain in the other, producing an orientation-independent J_γ .

The argument above, however, holds only when there is no additional noise present in the system. Additional noise, arising from, for example, a background count, has the adverse effect of masking small changes in intensity arising from small angular deflections of a perpendicularly oriented dipole, in a similar manner to how small changes of a co-oriented dipole are lost in the inherent Poisson noise.

Larger dipole deflections give rise to larger intensity changes in the detector, and thus when measuring dipole orientations that differ significantly from the critical angles, the background count becomes less relevant and the background free behaviour is restored. The extent of angular deviations considered to be significantly far from the critical orientations is naturally set by the strength of the background noise, hence explaining the widening of the information dip as S_0/D_b decreases.

Informational dips such as that discussed for a pair of crossed polarizers can also be seen for alternative polarimeter architectures, as shown in figure 4(b). Importantly, it should be noted that no dipole orientations give rise to complete loss of Fisher information, since each of these polarimeter configurations possesses additional arms. These additional arms are chosen such that the set of measurement states is not orthogonal such that a redundancy is introduced into the measurements. In turn, this implies that each detector suffers information dips at different dipole orientations. Consequently, the total information obtained is non-zero. For example, the polarimeter of Lara and Paterson (red dashed line) [29] possesses polarizers at $\pm 45^\circ$, in addition to polarizers at 0° and 90° . In a similar fashion to the crossed polarizers described above, the polarizers at $\pm 45^\circ$ suffer an information dip for dipoles orientated at $\pm 45^\circ$, but not for dipoles oriented at 0° or 90° . When considering the polarimeter as a whole, however, the effect of these dips is mitigated by the presence of the detection paths with crossed polarizers oriented at 0° and 90° , which yield non-zero information.

3.3. Dipolar crosstalk

In the preceding section, the image of an on-axis dipole was calculated and used to quantify the accuracy achievable in inferring the dipole's orientation. Introduction of a second, extraneous, off-axis dipole in the object plane, however, modifies the image plane distribution and can thus have consequences for any estimate of the first dipole's orientation, as shall now be analysed.

Consider first the image of an off-axis dipole. Displacement of a dipole to an off-axis position $\boldsymbol{\rho}_{\text{dp}} = (\rho_{\text{dp}}, \varphi_{\text{dp}}, 0)^T$ can be modelled by assuming shift invariance of the imaging system. Shift invariant imaging can be justified following the discussion in [26, 43], where the displacement is shown to introduce an additional phase term into the Debye–Wolf diffraction integral. The image of an off-axis dipole can, hence, be calculated using equation (1), whereby $\mathbf{E}_2^{\text{off-axis}}(\boldsymbol{\rho}_2) = \mathbf{E}_2^{\text{on-axis}}(\boldsymbol{\rho}_2 - \beta \boldsymbol{\rho}_{\text{dp}})$. The image field of the j th dipole (in this example only two dipoles will be considered such that $j = 1$ or 2), with moment $\mathbf{p}_j = p_0 (\cos \gamma_j, \sin \gamma_j, 0)^T$, can

then be expressed in the form

$$\mathbf{E}^{\text{dp}_j} = p_0 \begin{pmatrix} a_{1j+} \cos \gamma_j + a_{2j} \sin \gamma_j \\ a_{2j} \cos \gamma_j + a_{1j-} \sin \gamma_j \\ a_{3j} i \cos \gamma_j + a_{4j} i \sin \gamma_j \end{pmatrix}, \quad (21)$$

where

$$a_{1j\pm} = K_{0j}^A \pm K_{2j}^A \cos 2\Phi_j, \quad (22a)$$

$$a_{2j} = K_{2j}^A \sin 2\Phi_j, \quad (22b)$$

$$a_{3j} = -2K_{1j}^B \cos \Phi_j, \quad (22c)$$

$$a_{4j} = -2K_{1j}^B \sin \Phi_j. \quad (22d)$$

The index on the K integrals denotes the dependence on the radial coordinate $|\rho_2 - \beta \rho_{\text{dp}_j}|$ of the j th dipole, while $\Phi_j = \arctan[(y_2 - \beta y_{\text{dp}_j})/(x_2 - \beta x_{\text{dp}_j})]$.

The total intensity in the detector plane will, however, vary depending on the coherence properties of the light originating from the two dipoles. Two limiting cases will be considered here in which the light from the dipoles is either fully incoherent or fully coherent. The former situation may arise, for example, if imaging single fluorescent molecules, e.g. in fluorescence microscopy [44], where the inherently random nature of the excitation and re-emission process results in incoherent radiation, such that *intensities*, or equivalently Stokes parameters, add in the image plane. Alternatively, if imaging two dipoles induced by a coherent field, as may arise in the scattering of light from gold beads, or other small scatterers [45, 46], the dipoles radiate coherently, meaning that *field vectors* sum in the image plane.

Detection is assumed to be performed by a scanning point polarimeter comprising two polarizers oriented at $\vartheta_1 = 0^\circ$ and $\vartheta_2 = 90^\circ$, i.e. horizontally and vertically crossed polarizers as described in the preceding section. Strictly, the presence of a non-zero longitudinal field component for off-axis dipoles necessitates a full 3D treatment, whereby generalized Stokes vectors become 9×1 vectors [47]. The instrument matrix for the crossed polarizers scenario can then be shown to be given by

$$\mathbb{T} = \begin{pmatrix} \frac{2}{3} & \frac{1}{2} & 0 & 0 & 0 & 0 & 0 & 0 & -\frac{1}{2\sqrt{3}} \\ \frac{2}{3} & -\frac{1}{2} & 0 & 0 & 0 & 0 & 0 & 0 & -\frac{1}{2\sqrt{3}} \end{pmatrix}. \quad (23)$$

Accordingly, the detected intensity vector (as still found using $\mathbf{D} = \mathbb{T}\mathbf{S}/N$) is given by (once more neglecting background readings)

$$\mathbf{D}^{\text{inc}} = \frac{1}{2} \begin{pmatrix} |E_x^{\text{dp}_1}|^2 + |E_x^{\text{dp}_2}|^2 + |E_z^{\text{dp}_1}|^2 + |E_z^{\text{dp}_2}|^2 \\ |E_y^{\text{dp}_1}|^2 + |E_y^{\text{dp}_2}|^2 + |E_z^{\text{dp}_1}|^2 + |E_z^{\text{dp}_2}|^2 \end{pmatrix} \quad (24)$$

for the incoherent dipole case or alternatively by

$$\mathbf{D}^{\text{coh}} = \frac{1}{2} \begin{pmatrix} |E_x^{\text{dp}_1} + E_x^{\text{dp}_2}|^2 + |E_z^{\text{dp}_1} + E_z^{\text{dp}_2}|^2 \\ |E_y^{\text{dp}_1} + E_y^{\text{dp}_2}|^2 + |E_z^{\text{dp}_1} + E_z^{\text{dp}_2}|^2 \end{pmatrix} \quad (25)$$

for coherently radiating dipoles.

To evaluate the extent of crosstalk between the dipoles when attempting to infer the orientation of one dipole in the presence of Poisson noise, the FIM is again calculated. The magnitude of the dipole moment p_0 is assumed to be known *a priori* for simplicity and hence so too is S_0 , such that

$$J_{\gamma_1}^{\nu}(\gamma_1, \gamma_2) = \frac{1}{D_1^{\nu}} \left(\frac{\partial D_1^{\nu}}{\partial \gamma_1} \right)^2 + \frac{1}{D_2^{\nu}} \left(\frac{\partial D_2^{\nu}}{\partial \gamma_1} \right)^2 \quad (26)$$

for $\nu = \text{coh}$ or inc , denoting the coherent and incoherent cases, respectively. Calculating $J_{\gamma_1}^{\nu}$ requires the derivatives

$$\begin{aligned} \frac{\partial D_1^{\text{inc}}}{\partial \gamma_j} = p_0[(a_{2j} \cos \gamma_j - a_{1j+} \sin \gamma_j)(a_{1j+} \cos \gamma_j + a_{2j} \sin \gamma_j) \\ + (a_{4j} \cos \gamma_j - a_{3j} \sin \gamma_j)(a_{3j} \cos \gamma_j + a_{4j} \sin \gamma_j)], \end{aligned} \quad (27)$$

$$\begin{aligned} \frac{\partial D_2^{\text{inc}}}{\partial \gamma_j} = p_0[(a_{2j} \cos \gamma_j + a_{1j-} \sin \gamma_j)(a_{1j-} \cos \gamma_j - a_{2j} \sin \gamma_j) \\ + (a_{4j} \cos \gamma_j - a_{3j} \sin \gamma_j)(a_{3j} \cos \gamma_j + a_{4j} \sin \gamma_j)], \end{aligned} \quad (28)$$

$$\begin{aligned} \frac{\partial D_1^{\text{coh}}}{\partial \gamma_j} = p_0[(a_{2j} \cos \gamma_j - a_{1j+} \sin \gamma_j)(a_{11+} \cos \gamma_1 + a_{12+} \cos \gamma_2 + a_{21} \sin \gamma_1 + a_{22} \sin \gamma_2) \\ + (a_{4j} \cos \gamma_j - a_{3j} \sin \gamma_j)(a_{31} \cos \gamma_1 + a_{32} \cos \gamma_2 + a_{41} \sin \gamma_1 + a_{42} \sin \gamma_2)], \end{aligned} \quad (29)$$

$$\begin{aligned} \frac{\partial D_2^{\text{coh}}}{\partial \gamma_j} = p_0[(a_{1j-} \cos \gamma_j - a_{2j} \sin \gamma_j)(a_{21} \cos \gamma_1 + a_{22} \cos \gamma_2 + a_{11-} \sin \gamma_1 + a_{12-} \sin \gamma_2) \\ + (a_{4j} \cos \gamma_j - a_{3j} \sin \gamma_j)(a_{31} \cos \gamma_1 + a_{32} \cos \gamma_2 + a_{41} \sin \gamma_1 + a_{42} \sin \gamma_2)]. \end{aligned} \quad (30)$$

Examining the incoherent dipole case first, it is noted that the derivative terms, $\partial D_i^{\text{inc}}/\partial \gamma_1$, are independent of γ_2 and ρ_{dp_2} , while the additive terms, $|E_{\mu}^{\text{dp}_2}|^2$, ($\mu = x, y, z$) in equation (24) are independent of γ_1 and ρ_{dp_1} . As such, the second dipole acts as a background source. For all positions and orientations of the second dipole with a non-zero intensity at the detection point, information dips akin to those discussed in the single-dipole example above are introduced into the performance characteristics of any estimator for $\gamma_1 = 0^\circ$ or 90° .

With respect to coherent dipoles, consider briefly the limiting case in which the second dipole is moved to infinity, i.e. $\rho_2 \rightarrow \infty$. The functional dependence of the K integrals of equations (2) implies that $\{a_{12\pm}, a_{22}, a_{32}, a_{42}\} \rightarrow 0$ as $\rho_2 \rightarrow \infty$. Under these circumstances,

$$\begin{aligned} \frac{\partial D_1^{\text{coh}}}{\partial \gamma_1} \rightarrow p_0[(a_{21} \cos \gamma_j - a_{11+} \sin \gamma_1)(a_{11+} \cos \gamma_1 + a_{21} \sin \gamma_1) \\ + (a_{41} \cos \gamma_1 - a_{31} \sin \gamma_1)(a_{31} \cos \gamma_1 + a_{41} \sin \gamma_1)] = \frac{\partial D_1^{\text{inc}}}{\partial \gamma_1}, \end{aligned}$$

$$\begin{aligned} \frac{\partial D_2^{\text{coh}}}{\partial \gamma_1} \rightarrow p_0[(a_{11-} \cos \gamma_1 - a_{21} \sin \gamma_1)(a_{21} \cos \gamma_1 + a_{11-} \sin \gamma_1) \\ + (a_{41} \cos \gamma_1 - a_{31} \sin \gamma_1)(a_{31} \cos \gamma_1 + a_{41} \sin \gamma_1)] = \frac{\partial D_2^{\text{inc}}}{\partial \gamma_1}, \end{aligned}$$

whereupon it is seen that the coherent and incoherent cases exhibit the same behaviour for large dipole separations.

Limiting forms of $J_{\gamma_1}^v$ can also be derived when the second dipole is at a finite distance from the first, which shall now be assumed to again be located on-axis. Of significance is the form of equation (26) when \mathbf{p}_1 and \mathbf{p}_2 are parallel or perpendicular, since these configurations represent the two extreme configurations. Furthermore, the cases when \mathbf{p}_1 lies parallel or at 45° to the transmission axis of one of the analysing polarizers will be considered. Expressions for $J_{\gamma_1}^v(\gamma_1, \gamma_2)$ are hence now given when $\gamma_1 = 0$ for $\gamma_2 = 0$ and $\pi/2$ and also for $\gamma_1 = \pi/4$ and $\gamma_2 = \pm\pi/4$. For the incoherent case

$$J_{\gamma_1}^{\text{inc}}(0, 0) = J_{\gamma_1}^{\text{inc}}\left(0, \frac{\pi}{2}\right) = 0, \quad (31a)$$

$$J_{\gamma_1}^{\text{inc}}\left(\frac{\pi}{4}, \pm\frac{\pi}{4}\right) = \frac{J_{\gamma}^{\text{max}}}{2} \left[\frac{a_{11+}^2}{a_{11+}^2 + (a_{12+} \pm a_{22})^2 + (a_{32} \pm a_{42})^2} + \frac{a_{11-}^2}{a_{11-}^2 + (a_{22} \pm a_{12-})^2 + (a_{32} \pm a_{42})^2} \right], \quad (31b)$$

where the expected information loss at $\gamma_1 = 0^\circ$ and 90° is clearly evident. Coherent superposition of the radiated dipole fields yields

$$J_{\gamma_1}^{\text{coh}}(0, 0) = J_{\gamma}^{\text{max}} \frac{a_{22}^2}{a_{22}^2 + a_{32}^2}, \quad (32a)$$

$$J_{\gamma_1}^{\text{coh}}\left(0, \frac{\pi}{2}\right) = J_{\gamma}^{\text{max}} \frac{a_{12-}^2}{a_{12-}^2 + a_{42}^2}, \quad (32b)$$

$$J_{\gamma_1}^{\text{coh}}\left(\frac{\pi}{4}, \pm\frac{\pi}{4}\right) = \frac{J_{\gamma}^{\text{max}}}{2} \left[\frac{(a_{11+} + a_{12+} \pm a_{22})^2}{(a_{11+} + a_{12+} \pm a_{22})^2 + (a_{32} \pm a_{42})^2} + \frac{(a_{22} + a_{11-} \pm a_{12-})^2}{(a_{22} + a_{11-} \pm a_{12-})^2 + (a_{32} \pm a_{42})^2} \right]. \quad (32c)$$

Inspection of the denominators in equations (32) reveals that the longitudinal field component arising in the image plane from the extraneous dipole acts as a background source, a result that also holds for more general configurations (if the dipole of interest is located on axis). Informational losses, therefore, can once more result. Since the second lens is, however, practically of low NA, this background term is small and the dips correspondingly narrow.

Dropping the longitudinal background term thus allows the interference effects for coherent dipoles to be considered more closely. By the evaluation of equation (26) it can be shown that

$$J_{\gamma_1}^{\text{coh}}(\gamma_1, \gamma_2) = \frac{2p_0^2 K_{01}^A{}^2}{h\nu} = J_{\gamma}^{\text{max}}, \quad (33)$$

for all dipole configurations. The presence of a second dipole is thus seen to not affect $J_{\gamma_1}^{\text{coh}}$. That said, a bias, in general dependent on γ_1 , γ_2 and ρ_{dp_2} , is introduced into an estimator, with a resulting increase in the variance and the mean squared error [48]. As the interfering dipole is gradually moved to larger distances the magnitude of this bias decreases, so as to restore the single-dipole results of section 3.2.

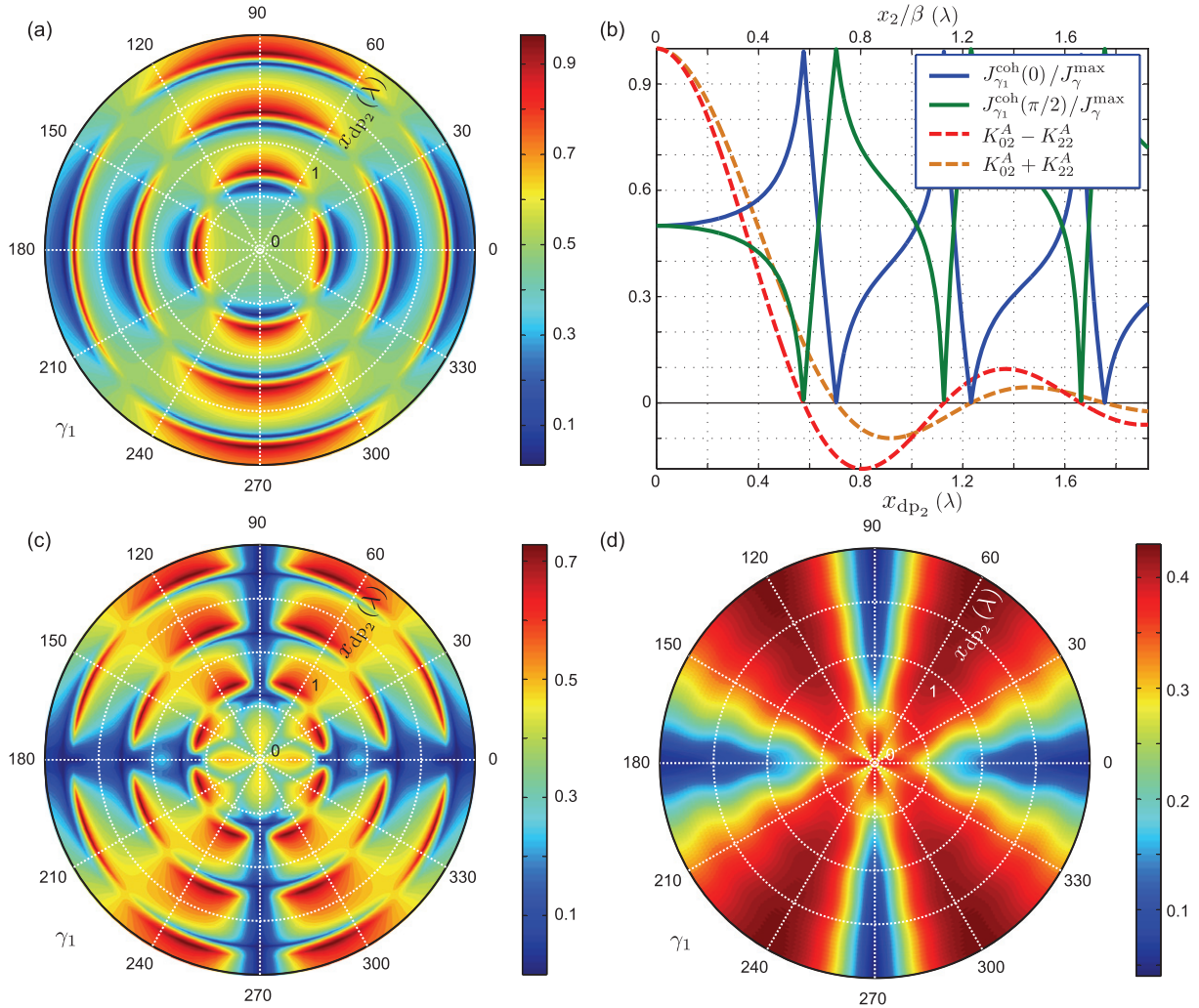


Figure 5. (a) The calculated normalized Bayesian Fisher information $J_{\gamma_1}^{\text{coh}}$ for estimating the orientation of an on-axis dipole in the presence of a second extraneous dipole located at $\rho_{\text{dp}_2} = (x_{\text{dp}_2}, 0, 0)$ as a function of γ_1 . (b) Line plots of normalized Fisher information for $\gamma_1 = 0^\circ$ and 90° as a function dipole separation. For reference, plots of $K_{02} \pm K_{22}$ are also shown. (c) The same as (a), but a further background intensity count D_b is introduced into the detection process, where $S_0/D_b = 10^2$. (d) The same as (c), albeit including detector scanning in the image plane over a square field of view with a spatial extent of $6 \times 0.61\lambda/\text{NA}_2$. The normalization factor used in (d) is given by $\int_{\Omega_{\text{im}}} J_{\gamma}^{\text{max}}(\rho_2) d\rho_2 = \frac{2p_0^2}{h\nu} \int_{\Omega_{\text{im}}} K_{01}^A{}^2(\rho_2) d\rho_2$.

Removal of the estimator bias could be approached by a reformulation of the problem as that of the joint estimation of (γ_1, γ_2) , in which the orientation of the second dipole is treated as a nuisance parameter. To illustrate the general performance that can be expected, a Bayesian viewpoint is adopted in which the orientation of the second dipole is assumed to obey a uniform probability density function, i.e. $f_{\Gamma_2}(\gamma_2) = 1/2\pi$, and the Fisher information for inference of

γ_1 is calculated as a function of dipole separation and γ_1 . The second dipole is assumed to lie on the positive x -axis in object space and the same imaging parameters as those assumed in section 3.2 are used.

When considering the coherent, zero background results ($D_b = 0$) shown in figure 5(a), it is also useful to consider figure 5(b), which shows the variation of $J_{\gamma_1}^{\text{coh}}(\gamma_1)$ with dipole separation, $\rho_{\text{dp}_2} = x_{\text{dp}_2}$, for $\gamma_1 = 0^\circ$ and 90° (solid lines). Plots of $K_{02}^A(\rho_2) \pm K_{22}^A(\rho_2)$ (normalized such that $K_{02}^A(0) = 1$) are also shown (dashed lines). These latter plots correspond to the variation of $E_x^{\text{dp}_2}(\rho_2)$ and $E_y^{\text{dp}_2}(\rho_2)$, respectively. Peaks in $J_{\gamma_1}^{\text{coh}}(0)$ are seen to correspond to zeros in $E_x^{\text{dp}_2}(\rho_2)$, while maxima in $J_{\gamma_1}(\pi/2)$ correspond to zeros in $E_y^{\text{dp}_2}(\rho_2)$. Such a situation can be understood by first noting that an x -oriented dipole yields zero intensity in D_2 when the second dipole is absent. The presence of a second dipole hence introduces noise into D_2 when $E_y^{\text{dp}_2}(\rho_2) \neq 0$, thus destroying the ability of an observer to identify the zero signal from the first dipole, in an analogous manner to the formation of informational dips. The scenario is similar for a y -oriented dipole, albeit the role of the detectors is reversed. A peak in $J_{\gamma_1}^{\text{coh}}(0)$ also corresponds to a minimum in $J_{\gamma_1}^{\text{coh}}(\pi/2)$ (and vice versa), by similar arguments.

When an independent background count D_b is introduced, zero Fisher information is seen for x - and y -oriented dipoles regardless of the position or angle of the second dipole as shown in figure 5(c), where the ratio $S_0/D_b = 10^2$ was assumed. Oscillations in the Fisher information as the dipole separation is increased, originally seen for the non-zero background case, are still exhibited, although the modulation of the oscillations is reduced. The extent of modulation is reduced since the information dips are broadened by the background count, hence washing out sharp variations. As D_b is further increased, this modulation reduces to a more uniform behaviour.

Scanning the polarimetric detector in the image plane and hence estimating molecule orientation from an extended image, however, also act to suppress informational oscillations, as shown in figure 5(d). While the informational dips at $\gamma_1 = 0^\circ$ and 90° are still present, the polarization variation of the image field helps to overcome informational losses introduced from inference from zero intensities in one or more detectors.

4. Conclusions

Principally, this study aimed to evaluate the precision limits when estimating the orientation of single molecules, as inferred from polarimetric measurements. To do so, the performance of a simple polarization microscope imaging a single molecule, modelled as an electric dipole emitter, was considered. Furthermore, a number of polarization measurement architectures were evaluated when attempting to estimate the molecule's transverse orientation based on a metric derived from Fisher information. While it was found that when attempting to determine the orientation of a single dipole a background free, crossed polarizer configuration (as is common in fluorescence anisotropy studies) performs well, informational losses at particular (although highly predictable) orientations were seen to occur when additional noise sources are introduced. Information losses of this nature were also seen in more complex architectures found in the literature. Greater redundancy can be introduced into these configurations by the use of a set of non-orthogonal measurement states, which can in turn reduce the significance of information dips. Fundamentally, it was found that, on average, a precision of 0.5 radian is achievable per photon. Due to the photon numbers achievable from different fluorescent dyes,

the importance of correct dye selection in obtaining a desired precision is evident, as too are efficient optical design and high-quality detectors. It is important to note that the analysis given in this paper is based on a fully rigorous electromagnetic imaging model. As such, precision losses that may arise from corrections made for polarization effects (see, e.g., [49–51]) are automatically factored into the quoted precision of 0.5 radian per photon. Furthermore, this precision does not include further gains that may be achieved by the use of squeezed optical states or by exploiting the anti-bunched statistics of single-molecule emission. For comparison, an angular precision of 0.2° , 2° and 2° was quoted by Ha *et al* [14], Prummer *et al* [33] and Aguet *et al* [17], who, respectively, used polarization modulation, optical polarization tomography and defocused image acquisition to infer molecular orientation. Prummer *et al* [33] quote a shot-limited value, while that of Aguet *et al* [17] is found using the CRLB and hence both are directly comparable to the results given in this work. Given an average precision of 0.5 radian per photon, a comparable precision could be achieved using complete polarization measurements with only ~ 14 photons, which is easily achievable even in high-loss systems.

Multiple molecules present in a detection volume are well known to give rise to large errors in localization techniques. Precision losses in the domain of orientational measurements were thus also investigated by considering the introduction of a second extraneous dipole. If incoherently radiating with respect to the first, this second molecule acts as a background source, thus having a detrimental effect on the measurement process, such as inducing information dips as found in the single molecule case. Although similar effects can be seen for a second coherently radiating dipole, the extent of performance degradation becomes dependent on the relative configuration of the two dipoles producing a more complex behaviour. In essence, however, all informational losses are seen to occur when inference is based on null readings, due to their susceptibility to any additional perturbations. If estimation of the molecular orientation is based on an image formed (e.g., by the use of a scanning microscope), a reduction in the complexity of the dipole crosstalk attributes is seen, partly due to the averaging introduced in such measurements, but also due to the larger number of measurements taken.

Acknowledgment

This work was funded by the European Union via the SURPASS project (grant no. 224226).

References

- [1] Hess S T, Girirajan T P K and Mason M D 2006 Ultra-high resolution imaging by fluorescence photoactivation localization microscopy *Biophys. J.* **91** 4258–72
- [2] Rust M J, Bates M and Zhuang X 2006 Sub-diffraction-limit imaging by stochastic optical reconstruction microscopy (STORM) *Nat. Methods* **3** 793–6
- [3] Shroff H, Galbraith C G, Galbraith J A and Betzig E 2008 Live-cell photoactivated localization microscopy of nanoscale adhesion dynamics *Nat. Methods* **5** 417–23
- [4] Hwang J, Pototschnig M, Lettow R, Zumofen G, Renn A, Götzinger S and Sandoghdar V 2009 A single-molecule optical transistor *Nature* **460** 76–80
- [5] Mortensen K I, Churchman L S, Spudich J A and Flyvbjerg H 2010 Optimized localization analysis for single-molecule tracking and super-resolution microscopy *Nat. Methods* **7** 377–81
- [6] Brokmann X, Ehrensperger M-V, Hermier J-P, Triller A and Dahan M 2005 Orientational imaging and tracking of single CdSe nanocrystals by defocused microscopy *Chem. Phys. Lett.* **406** 210–4

- [7] Spille J-H, Zürn A, Hoffmann C, Lohse M J and Harms G S 2011 Rotational diffusion of the α_{2a} adrenergic receptor revealed by FIAsh labeling in living cells *Biophys. J.* **100** 1139–48
- [8] Dale R E and Hopkins S C 1999 Model-Independent analysis of the orientation of fluorescent probes with restricted mobility in muscle fibers *Biophys. J.* **76** 1606–18
- [9] Pavičić D, Lee K F, Rayner D M, Corkum P B and Villeneuve D M 2007 Direct measurement of the angular dependence of ionization for N_2 , O_2 , and CO_2 in intense laser fields *Phys. Rev. Lett.* **98** 243001
- [10] Sick B, Hecht B and Novotny L 2000 Orientational imaging of single molecules by annular illumination *Phys. Rev. Lett.* **85** 4482–5
- [11] Dickson R M, Norris D J and Moerner W E 1998 Simultaneous imaging of individual molecules aligned both parallel and perpendicular to the optic axis *Phys. Rev. Lett.* **81** 5322–5
- [12] Patra D, Gregor I and Enderlein J 2004 Image analysis of defocused single molecule images for three dimensional molecular orientation studies *J. Phys. Chem. A* **108** 6836
- [13] Foreman M R, Macías Romero C and Török P 2008 Determination of the three dimensional orientation of single molecules *Opt. Lett.* **33** 1020–2
- [14] Ha T, Enderle T, Chemla D S, Selvin P R and Weiss S 1996 Single molecule dynamics studied by polarization modulation *Phys. Rev. Lett.* **77** 3979–82
- [15] Gould T J, Gunewardene M S, Gudheti M, Verkhusha V V, Yin S-R, Gosse J A and Hess S T 2008 Nanoscale imaging of molecular positions and anisotropies *Nat. Methods* **5** 1027–30
- [16] Pavani S R P, DeLuca J G and Piestun R 2009 Polarization sensitive, three-dimensional, single-molecule imaging of cells with a double-helix system *Opt. Express* **17** 19644–55
- [17] Aguet F, Geissbühler S, Märki I, Lasser T and Unser M 2009 Super-resolution orientation estimation and localization of fluorescent dipoles using 3-D steerable filters *Opt. Express* **17** 6829–48
- [18] Ober R J, Ram S and Ward E S 2004 Localization accuracy in single-molecule microscopy *Biophys. J.* **86** 1185–200
- [19] Ram S, Ward E S and Ober R J 2006 Beyond Rayleigh's criterion: a resolution measure with application to single-molecule microscopy *Proc. Natl Acad. Sci. USA* **103** 4457–62
- [20] Foreman M R and Török P 2010 Information and resolution in electromagnetic optical systems *Phys. Rev. A* **82** 043835
- [21] Foreman M R, Sherif S S and Török P 2007 Photon statistics in single molecule orientational imaging *Opt. Express* **15** 13597–606
- [22] Qu X, Wu D, Mets L and Scherer N F 2004 Nanometer-localized multiple single molecule fluorescence microscopy *Proc. Natl Acad. Sci. USA* **101** 11298–303
- [23] Ta H, Wolfrum J and Herten D-P 2009 An extended scheme for counting fluorescent molecules by photon-antibunching *Laser Phys.* **20** 119–24
- [24] Foreman M R and Török P 2010 Computational methods in vectorial imaging *J. Mod. Opt.* **57** 1–26
- [25] Török P, Varga P, Laczik Z and Booker G R 1995 Electromagnetic diffraction of light focused through a planar interface between materials of mismatched refractive indices: an integral representation *J. Opt. Soc. Am. A* **12** 325–32
- [26] Török P, Higdon P D and Wilson T 1998 On the general properties of polarised light conventional and confocal microscopes *Opt. Commun.* **148** 300–15
- [27] Oldenbourg R and Mei G 1995 New polarized light microscope with precision universal compensator *J. Microsc.* **180** 140–7
- [28] Azzam R 1985 Arrangement of four photodetectors for measuring the state of polarization of light *Opt. Lett.* **10** 309–11
- [29] Lara D and Paterson C 2009 Stokes polarimeter optimization in the presence of shot and Gaussian noise *Opt. Express* **17** 21240–9
- [30] Azzam R M A and Bashara N M 1982 Division-of-amplitude photopolarimeter (DOAP) for the simultaneous measurement of all four Stokes parameters of light *J. Mod. Opt.* **29** 685–9
- [31] Compain E and Drevillon B 1998 Broadband division-of-amplitude-polarimeter based on uncoated prisms *Appl. Opt.* **37** 5938–44

- [32] Lakowicz J R 2006 *Principles of Fluorescence Spectroscopy* 3rd edn (Berlin: Springer)
- [33] Prummer M 2003 Three-dimensional optical polarization tomography of single molecules *J. Chem. Phys.* **118** 9824–9
- [34] Fourkas J 2001 Rapid determination of the three-dimensional orientation of single molecules *Opt. Lett.* **26** 211–3
- [35] Chung I, Shimizu K T and Bawendi M G 2001 Room temperature measurements of the 3D orientation of single CdSe quantum dots using polarization microscopy *Proc. Natl Acad. Sci. USA* **100** 405–8
- [36] Nee T, Nee S, Yang D and Huang Y 2008 Scattering polarization by anisotropic biomolecules *J. Opt. Soc. Am. A* **25** 1030–8
- [37] Cramér H 1946 *Mathematical Methods of Statistics* (Princeton, NJ: Princeton University Press)
- [38] Rao C 1945 Information and the accuracy attainable in the estimation of statistical parameters *Bull. Calcutta Math. Soc.* **37** 81–9
- [39] Fisher R A 1922 On the mathematical foundations of theoretical statistics *Philos. Trans. R. Soc. Lond.* **222** 309–68
- [40] Frieden B R 1998 *Physics from Fisher Information: A Unification* (Cambridge: Cambridge University Press)
- [41] Foreman M R, Macías Romero C and Török P 2000 *A priori* information and optimisation in polarimetry *Opt. Express* **16** 15212–227
- [42] Foreman M R, Sherif S S, Munro P R T and Török P 2008 Inversion of the Debye–Wolf diffraction integral using an eigenfunction representation of the electric fields in the focal region *Opt. Express* **16** 4901–17
- [43] Munro P R T and Török P 2007 Calculation of the image of an arbitrary vectorial electromagnetic field *Opt. Express* **15** 9293–307
- [44] Higdon P D, Török P and Wilson T 1999 Imaging properties of high aperture multiphoton fluorescence scanning microscopes *J. Microsc.* **193** 127–41
- [45] Török P, Higdon P D and Wilson T 1998 Theory for confocal and conventional microscopes imaging small dielectric scatterers *J. Mod. Opt.* **45** 1681–98
- [46] van de Hulst H C 1981 *Light Scattering by Small Particles* (New York: Dover)
- [47] Foreman M R 2010 Informational limits in optical polarimetry and vectorial imaging *PhD thesis* Imperial College, London
- [48] Scharf L L 1991 *Statistical Signal Processing: Detection, Estimation, and Time Series Analysis* (Reading, MA: Addison-Wesley)
- [49] Axelrod D 1989 Total internal reflection fluorescence microscopy *Methods Cell Biol.* **30** 245–70
- [50] Stallinga S and Rieger B 2010 Accuracy of the Gaussian Point Spread Function model in 2D localization microscopy *Opt. Express* **18** 24461–76
- [51] Bahlmann K and Hell S 2000 Depolarization by high aperture focusing *Appl. Phys. Lett.* **77** 612–4